Preparation and Characterization of Crosslinked PVAL Membranes Loaded with Boehmite Nanoparticles for Fuel Cell Applications

Paula Nunes Oliveira,[1] Margarida Catarino,[2] Carmem Maria Oliveira Müller,[1] Lúcia Brandão,[2] David Alfredo Pacheco Tanaka,[2] José Roberto Bertolino,[1] Adélio M. Mendes,[2] Alfredo Tibúrcio N. Pires[1]

[1]Grupo de Estudo em Materiais Poliméricos, POLIMAT, UFSC, Florianópolis, Santa Catarina, Brazil
[2]LEPAE, DEQ, Universdade do Porto, Faculdade de Engenharia, Portugal
Correspondence to: P. N. Oliveira (Email: paula_qmc@yahoo.com.br)

ABSTRACT: Composite proton conducting membranes were prepared by doping the membrane, prepared by crosslinking poly(vinyl alcohol) with sulfosuccinic acid (SSA), with boehmite [aluminum oxyhydroxide or γ-AlO(OH)]. The effect of the SSA and boehmite content on the membrane performance was studied and the results showed that the values for the ion exchange capacity (IEC) of the membranes were in the range of 0.45–4.80 mmol g^{-1}, the water content and the Young's modulus were dependent on the amount of SSA and nanoparticles. The proton conductivity was in the range of 10^{-4} to 10^{-2} S cm^{-1} at 25°C and was directly related to the quantity of sulfonate groups present in the membrane, while the hydrogen permeability at 30°C was in the range of 10^{-13} to 10^{-12} mol cm s^{-1} cm^{-2} bar. The proton exchange membrane fuel cell tests indicated that the composite membranes have good proton conductivity and very low hydrogen permeability. © 2013 Wiley Periodicals, Inc. J. Appl. Polym. Sci. **2014**, *131*, 40148.

INTRODUCTION

Fuel cells are one of the clean alternatives to fossil fuels, which have the potential to produce energy with low emissions and high efficiency. They convert directly the chemical energy of a fuel into electrical power. When the fuel is hydrogen, the products generated are water, heat, and energy. PEMFC can be used in power generation systems for on-site electricity generation, in transportation and in portable devices such as cell phones and computers, offering an attractive balance between energy storage and volume size.

The proton-conducting membrane is the "heart" of the fuel cell, and must fulfil several requirements simultaneously, that is: high proton conductivity with electrical isolation, adequate mechanical, thermal, and chemical stability, and low fuel permeability. The most commonly used membrane is a perfluorinated membrane, Nafion, developed by DuPont.[1,2] However, Nafion membranes present some limitations relating to this application, such as low ionic conductivity at low humidity, susceptibility to degrade at high temperatures and high cost.[3]

Several membranes have been evaluated as alternatives to Nafion membranes for PEMFC applications. Progress have been

achieved with membranes prepared from modified aromatic polymers such as sulfonate poly(arylene ether sulfone),[4] sulfonate poly (ether ether ketone),[5–7] and sulfonate poly(arylene ether ketone).[8,9] Experiments have also been performed using cheap polymers such as polystyrene ethylene butylene polystyrene (PSEBS),[10] and poly(vinyl alcohol) (PVAL),[11,12] which can be converted to sulfonated polymers. Some basic polymers such as poly(2,5-benzimidazole) (ABPBI)[13] and polybenzimidazole (PBI)[14] have also been tested.

Among the aforementioned polymers, PVAL is a polymer that presents a high affinity for water and has been studied as a membrane because it offers good film-forming and chemical-resistance properties.[15,16] The high density of —OH functional groups in the polymer chain confers hydrophilic properties and selectivity, that can be improved through modification of the polymer chemical structure by crosslinking, grafting, etc. One agent that can be used for the modification of the polymeric chain through the inclusion of acid groups is sulfosuccinic acid, which besides having two carboxylic acid groups also has a sulfonic acid group. Rhim et al. prepared membranes by crosslinking of PVAL with SSA and observed proton conductivity values in the range of 10^{-3} to 10^{-2} S cm^{-1}.[11] However, the membranes formed by

PVAL modified with SSA presented a relatively low working temperature (at around 80°C) due to the dependence on water to protons transportation (similar to Nafion).

A great number of alternative strategies have been investigated for the development of proton conducting membranes in dehydrating environments, i.e., elevated temperatures and reduced relative humidity, such as hybrid organic–inorganic membranes. These composite membranes are characterized by the incorporation on a nanometric scale of inorganic (fillers),[17] in which the filler-polymer interaction can range from strong (covalent and ionic) bonds to weak physical interactions. The addition of an inorganic material in the polymeric membrane often improves the chemical and mechanical stability and retains the water at higher temperatures thus increasing the membrane working temperature.[18,19] Many inorganic fillers have been studied: TiO_2,[20,21] ZrO_2,[18,22] $Zr(HPO_4)_2.nH_2O$ (ZrP),[23,24] zirconium phosphate-sulfo phenylene phosphonates,[25] SiO_2,[26] and so forth. The results reported in the literature confirm that these fillers are indeed effective in improving in the thermal stability of the composite membranes, increasing the water retention at higher temperatures and improving the mechanical properties.[27] The inclusion of nanoparticles of SiO_2 in PVAL/SSA membranes was studied by Kim et al., who observed a reduction of free water ratio due to the presence of silica particles.[26]

Boehmite and diaspore are the two mineralogical forms of alumina monohydrate ($Al_2O_3.H_2O$) or aluminum oxyhydroxide (AlO(OH)) and are the most abundant constituents of bauxite. In many cases, boehmite (γ-AlO(OH)) is the starting material in the synthesis of alumina phases.[28,29] These particles with high anisotropy can account for the additional improvement in the mechanical properties of polymers.[30,31] Some examples about incorporation of boehmite into polymers in order to obtain composite materials can be found in literature. The inclusion of colloidal boehmite rods in the polyeamine-6 was studied by Özdilek et al., and a mechanical reinforcement of the matrix was verified,[31] as well as in the boehmite–based polyethylene nanocomposites prepared *in situ* polymerization of ethylene in the boehmite presence.[32] On the other hand, the boehmite can also be applied to improve the thermal and the combustion properties, as shown by Monti and Camino, who reported a significant flame retardant effect of the nanosize boehmite particles in polyethersulfone (PES).[33] Zhang et al. showed an improvement on the thermal stability and flame retardant properties of the poly(ethylene terephtalate) (PET) with incorporation of nanoboehmite.[34]

In this article, the chemical and physical properties of PVAL/SSA membranes, loaded or not with γ-AlO(OH) or boehmite, were assessed and compared and the membranes loaded with boehmite, which showed the best properties to application as PEM had their performance evaluated in a fuel cell.

EXPERIMENTAL

Materials

Poly(vinyl alcohol) (PVAL) (99% hydrolyzed with molecular weight of 89,000 to 98,000 g mol^{-1}) and sulfosuccinic acid (SSA, 70% aqueous solution) were supplied by Sigma Aldrich

Table I. Chemical Composition and Molar Ratio of Investigated Membranes

Membrane code	PVAL/SSA (w/w)	PVAL/SSA (mol/mol)[a]
# 1	95/5	86/1
# 2	90/10	41/1
# 3	85/15	26/1
# 4	74/26	12/1
# 5	57/43	6/1
# 6	45/55	4/1

[a] Corresponding to moles of monomeric unit/SSA moles.

Chemical Co. Boehmite sol nanoparticles (10 wt % aqueous solution) with a size of 10 nm were provided by Kawaken Fine Chemicals. The products used to develop this study were not purified before usage.

Membrane Preparation

Aqueous 10 wt % PVAL solutions were prepared by dissolving dry PVAL in water and adding the SSA to the PVAL solution according to the quantities specified in Table I. The solution was stirred for 24 h and casted on a polystyrene plate at room temperature and a homogeneous membrane was obtained after solvent evaporation. The membrane was maintained at 90°C for 1.5 h to promote the crosslinking reaction. For the preparation of composite membranes nanoparticles of boehmite (5 and 10 wt % relative to the polymer mass) were inserted into PVAL aqueous solution. After 2 h stirring, SSA was added and the membranes were obtained by casting and submitted to the thermal treatment to promote the crosslinking reaction as described above, and afterwards the membranes were evaluated without additional treatment.

Characterization

The membranes were supported in silicon wafers and analyzed by Fourier transform infrared (FTIR) spectrometry, using a Nicolet Magna IR 860 Instrument (Thermo Nicolet, Madison, WI) operating within a range of 4000–400 cm^{-1}, at a 2 cm^{-1} spectral resolution by transmission mode. The SSA spectrum was obtained from aqueous solution (70% w/v).

The thermal stability of the membranes was evaluated using a thermogravimetric analyzer (TGA) (TGA50-Shimatzu). A constant temperature ramp rate of 10°C min^{-1} from room temperature up to 700°C under N_2 flow was applied. Before the analysis the membranes were maintained under vacuum for 24 h.

The TG analysis coupled with infrared spectroscopy was carried out using a TGA from Netzsch (model STA 449 F1 Jupiter) and a FTIR from Bruker (model TENSOR 27). Initially, the samples were maintained under vacuum for 24 h at room temperature. Then, the samples were submitted to a 10°C min^{-1} constant temperature heating rate from 40°C up to 700°C under N_2 flow of 20 mL min^{-1}. The gases generated during the heating were taken to FTIR by nitrogen stream and the spectroscopic analysis performed every 2 min.

Differential scanning calorimetry (DSC) measurements were performed using a DSC (TA-50 Shimatzu) equipped with a

cooling apparatus to determine the free water content of fully hydrated membranes. After cooling the sample with liquid nitrogen, the experiment began by heating the sample from $-80°C$ to $30°C$ using a $5°C$ min^{-1} heating rate. Nitrogen gas was used as the carrier gas at a flow rate of 50 mL min^{-1}. The crystallization and melting temperatures of freezable water adsorbed in the sample were determined from the temperature at the maximum point of the corresponding enthalpy peaks. The freezable water mass (W_c) was obtained through eq. (1):

$$W_c = \frac{q}{\Delta H} \qquad (1)$$

where ΔH is the melting enthalpy of freezable water, assumed to be same of the bulk water ($\Delta H = 333.5$ J g^{-1}), and q is the heat absorbed during the melting process. The q value was calculated using the area under the endothermic peak. The procedure to determine the amount of freezable water does not take into account the differences in the melting enthalpies of the different crystal structures of ice and thus the maximum relative error computing the freezable water is 6.6%.[35] The mass of nonfreezable bound water was obtained from the difference between the mass of absorbed water and the total absorbed free water in the membrane.

The dynamic mechanical analysis was performed using a DMA Q800-TA. Initially, the membranes of PVAL/SSA loaded and unloaded nanoparticles, 0.53 mm wide, were equilibrated at 100% relative humidity for 24 h. For the test strain deformation, samples were kept at $50°C$ for 2 min and then submitted to 0.01 N s^{-1} rate strength, in which the maximum force applied was 18 N. The Young's modulus was computed based on the average strain and stress values obtained from three determinations for each membrane formulation.

Water Uptake

The water uptake was determined gravimetrically and the membranes were previously-dried, weighed (W_{dry}) and immersed in water at room temperature. After 24 h, the membranes were taken out, the solvent on the surface was quickly removed and weighted (W_{wet}). The water uptake per sample gram was calculated by mass difference between wet and dried membranes ($W_{wet} - W_{dry}$) and normalized per gram of dried membranes.

Ion Exchange Capacity (IEC)

The IEC of the membranes was determined through acid–base titration. The dry membrane was immersed in 20 mL of saturated sodium chloride aqueous solution for 24 h in order to exchange protons for sodium ions. The acid released was subsequently titrated using a 0.01 mol L^{-1} sodium hydroxide solution and phenolphthalein as the indicator. IEC was calculated using eq. (2):

$$\text{IEC} = \frac{M.V}{W_{dry}} \qquad (2)$$

where M is the concentration of the titrant (mol L^{-1}), V is the added volume of titrant at the equivalent point (mL), and W_{dry} is the dry mass of the sample (g).

Conductivity

The conductivity was measured by AC electrochemical impedance spectroscopy in the frequency range of 1–500 kHz with

signal amplitude of 5 mV and derived from the high frequency intercept of the complex impedance with the real axis, using a two-electrode arrangement. Measurements were performed under 100% relative humidity at $25°C$.

The impedance measurements were carried out using a Zahner IM6 electrochemical workstation. The proton conductivity (σ) was obtained using the following eq. (3):

$$\sigma = \frac{l}{R.S} \qquad (3)$$

where σ is the proton conductivity (S cm^{-1}), l is the distance between the electrodes (thickness of membrane, cm), R is the impedance of membrane (Ω), and S is the surface area required for a proton to penetrate the membrane (electrode area) (cm^2).

Gas Permeation Measurements

The membrane permeation to hydrogen was determined by the time lag method and the experimental set-up used is described in detail in Ref. 36. The experiments were performed at $30°C$ and 75% relative humidity and prior to the test, the membranes were equilibrated with water at 75% relative humidity, for 12 h. The membranes denoted by #4, #5, and #6, loaded and unloaded with boehmite nanoparticles, had shown good results in the proton conductivity tests and had their gas permeation properties evaluated.

PEMFC Tests

The modified PVAL membranes were sandwiched between Toray carbon papers loaded with catalyst with an effective area of 5 cm^2, using a Pt loading of 0.5 mg_{Pt} cm^{-2} (10 wt % Pt/Vulcan, Electrochem S.A) at the anode and cathode. The PEMFC using with these membranes was operated at $50°C$ with a feed flow rate of 200 mL min^{-1} of hydrogen at 1 bar and 100% relative humidity, and 400 mL min^{-1} of air at 1 bar and 90% relative humidity. The PEMFC tests using reference Nafion 115 membrane were operated under identical conditions. Fuel cells were characterized by electrochemical impedance spectroscopy (EIS) and polarization curves.

RESULTS AND DISCUSSION

FTIR Spectroscopy

Figure 1 shows the infrared spectra for the PVAL membrane, SSA and PVAL/SSA membranes in the regions of 3800–2750 cm^{-1} and 1800–400 cm^{-1}. The PVAL membrane absorption spectrum shows the characteristic broad absorption bands at 3330 cm^{-1} (—OH stretching), at 2940 cm^{-1} (—CH_2 stretching), at 1433 cm^{-1} (C—H deformation) and at 1096 cm^{-1} (C—O stretching).[12,37] The absorption spectrum of SSA aqueous solution (70% w/v) exhibits a wider absorption band in the region of 3200–3600 cm^{-1} related to the O—H stretching vibration in —SO_3H, COOH and free water.[38] The absorption band observed at 1632 cm^{-1} is due to the —OH angular deformation mode from the water molecules bonded with the —SO_3^- group.[39] The carboxylic stretching centered at 1724 cm^{-1} (COOH), the asymmetric O=S—O stretching at 1167 cm^{-1}, the symmetric S—O stretching at 1041 cm^{-1} and at 860 cm^{-1} and the —CH_2— and C—H stretching at 2800–2900 cm^{-1} and 1300–1500 cm^{-1}, respectively are also visible in the spectrum of SSA.[11]
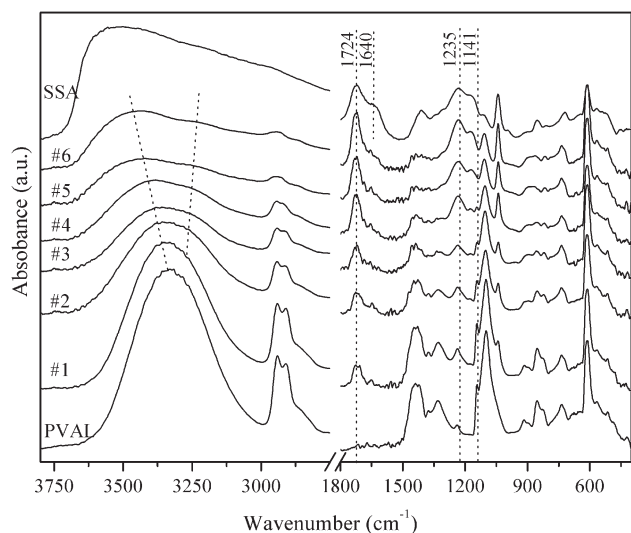
Figure 1. (A) Infrared spectra of SSA, PVAL, and PVAL/SSA membranes in the region of 3800–400 cm^{-1} (B). Numbers #1 to #6 denote membranes with composition as indicated in Table I.

Figure 3. Infrared spectrum of SSA, PVAL, and PVAL/SSA loaded with 10% of γ-AlO(OH) membranes in the region of 3800–400 cm^{-1}. Numbers #1 to #6 denote membranes with composition as indicated in Table I.

Intramolecular and intermolecular hydrogen bonding occur between PVAL chains due to high hydrophilic forces. The intensity of the absorption band at 1141 cm^{-1} in the PVAL is related with the polymeric chain crystalline portion. This band has been used as a tool to assess the PVAL structure, as it is a semi-crystalline synthetic polymer able to form different domains depending on several process parameters. Figure 1 shows that the intensity of band at 1141 cm^{-1} decreases as the sulfosuccinic acid content is increased in the membranes composition. The crystalline portion is dependent on the number of —OH groups from the PVAL precursor that decreases as esterification reaction progresses.[40,41] A esterification reaction scheme between the hydroxyl group of PVAL and the carboxyl group of sulfosuccinic acid is shown in Figure 2.

Large bands are observed between 3550 and 3200 cm^{-1} on the infrared spectra of the PVAL/SSA membranes (Figure 1). These are linked to the O—H stretching of the water molecules attached to the ionic domains and to the polar sites in the polymer. In this case is difficult to establish a direct correlation between the bands intensity due to overlapping. However, with an increase in the membrane SSA amount the wave number of the O—H stretching vibration shifts to a higher wave number (ca. 3400 cm^{-1}). This observation suggests that the hydrogen
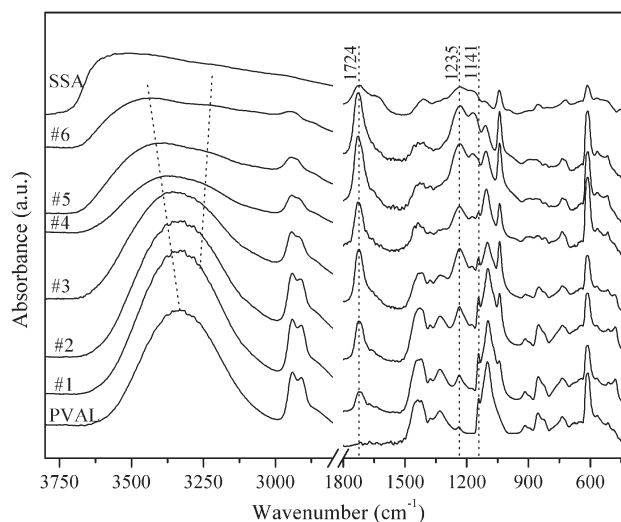
bonding between the —OH groups of PVAL shifted due to a decrease in the intramolecular interactions and also a new absorption component, which appears at higher wave numbers. It should be noted that the esterification reaction also decreases the number of free —OH groups in the PVAL and consequently the intensity of bands related with this group decreases.[36]

The absorption bands relative to boehmite (γ-AlO(OH)) overlap the sulfosuccinic acid bands in the region of 1500–1300 cm^{-1} and with the symmetric —CH$_2$ stretching at 2800–2900 cm^{-1}. The interaction between the PVAL and nanoparticles probably occurs by ionic interaction between the hydroxyl group from the PVAL and the —OH sites of the γ-AlO(OH). This interaction can cause significant changes in the dipole moment of —OH and —CO groups in the PVAL and consequently the intensity and the wave number of the absorption bands may change. Absorption band intensity can be influenced by the esterification reaction, which decreases the free —OH groups in the PVAL, and consequently decreases the bands intensity related with this group.[40] These characteristics related with absorption bands and relative intensity at 3000–3600 cm^{-1} spectra range were observed in Figure 3.
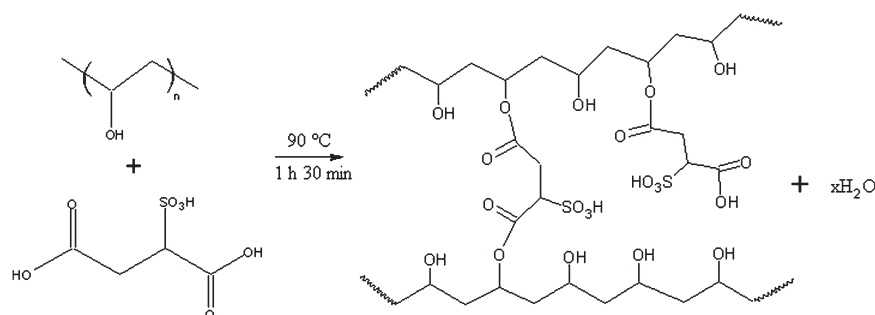

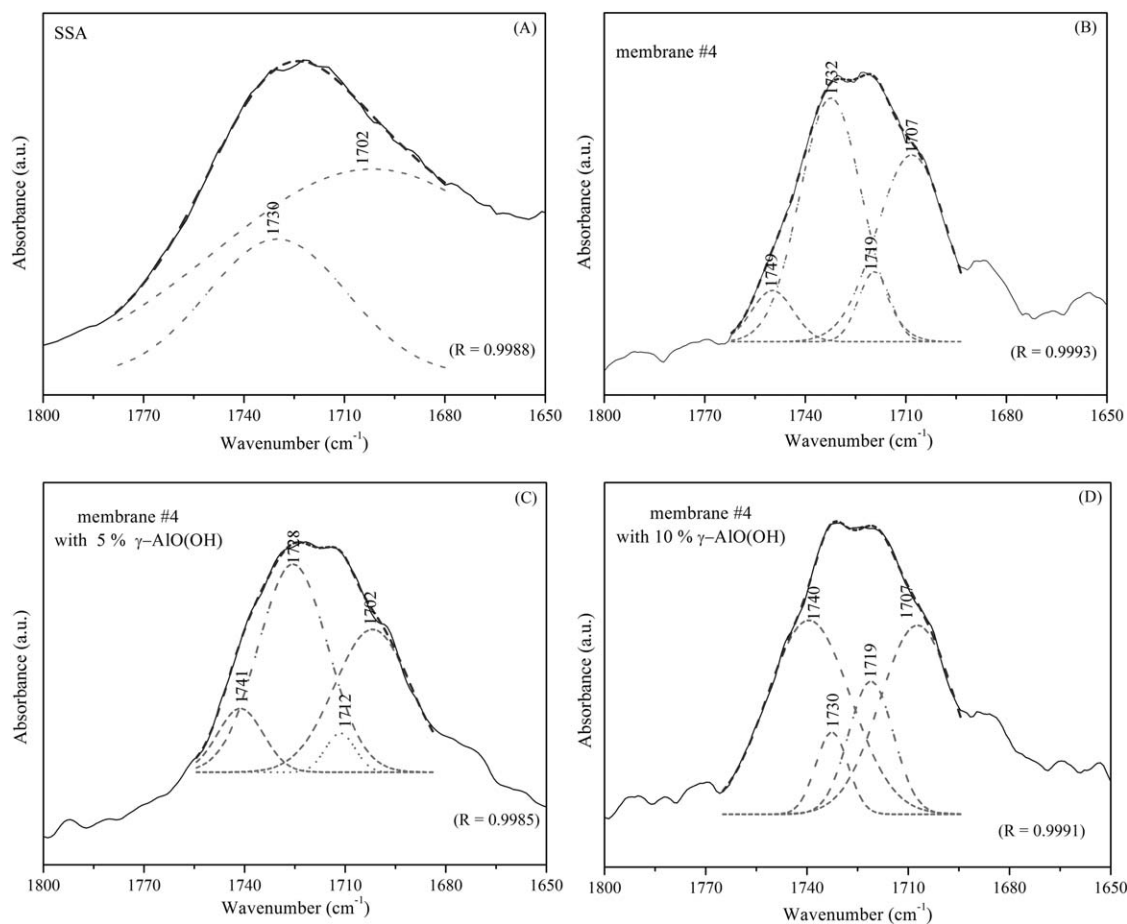**Figure 2.** Reaction scheme for PVAL/SSA crosslinking.

Figure 4. Deconvolution bands on the infrared spectra for (A) SSA and (B) membrane #4, and (C) membrane #4 loaded with 5%, and (D) loaded with 10 % of γ-AlO(OH).

In the spectrum of the SSA, two carboxylic groups contribute to the band centered at 1724 cm^{-1}. With the increasing of SSA amount, new contributions from the carboxylic groups appear at higher wave numbers, evidencing the formation of crosslinking between PVAL and SSA. Figure 4 shows the spectra deconvolution of the 1770–1680 cm^{-1} wave number range for SSA and of the 1765–1695 cm^{-1} wave number range for membrane #4, membrane #4 loaded with 5%, and loaded with 10% of boehmite. The deconvolution indicates that different carboxylic groups contribute to the absorption bands in these regions. The absorption bands at the higher wave number for membranes #4 are attributed to the carboxylic group with the weakest association with water molecules (i.e., the carboxylic group from the ester). On the other hand, bands at the lower wave numbers are attributed to the carboxylic group associated with water molecules. The bands deconvolution analysis was performed to all membranes and showed four bands in all cases, being this an indicative that a partial crosslinking reaction occurred.

The absorption band characteristic of the ester group (C—O stretching at 1235 cm^{-1}) for PVAL/SSA membranes loaded with boehmite can be observed in Figure 3. The changes in the infrared spectra suggest that the crosslinking reaction occurred between the hydroxyl groups of the PVAL and the carboxylic groups of the SSA and that the nanoparticles presence did not interfere in the reaction between PVAL and SSA. The relative intensity of these characteristic bands increases as the content of sulfosuccinic acid increases. Although this provided clear evidence of crosslinking, it is difficult to know correctly the crosslinking degree using FTIR spectrometry; thus other characterization techniques were performed and are discussed below.

Thermal Analysis

The thermal stability of crosslinked PVAL/SSA membranes loaded or unloaded with boehmite nanoparticles was investigated by TGA. The thermogravimetric curves of the three types of membranes presented the same profile, with different residual mass amount because of SSA and to inorganic material content. The thermogravimetric curves in Figure 5(A) show that membranes have three main degradation stages, as observed in the DTG curves [Figure 5(B)]. These thermogravimetric curves showed the same characteristics for similar systems found in the Ref. 11, 42, in which the weight loss at around 200°C is mostly attributable to the adsorbed water loss. The second (at around 300°C) and the third (at around 480°C) weight losses are related to the degradation membrane components. The weight losses in these two steps are directly associated with the SSA amount in the membrane. A rise in SSA content causes increased weight loss at around 300°C, and consequently a
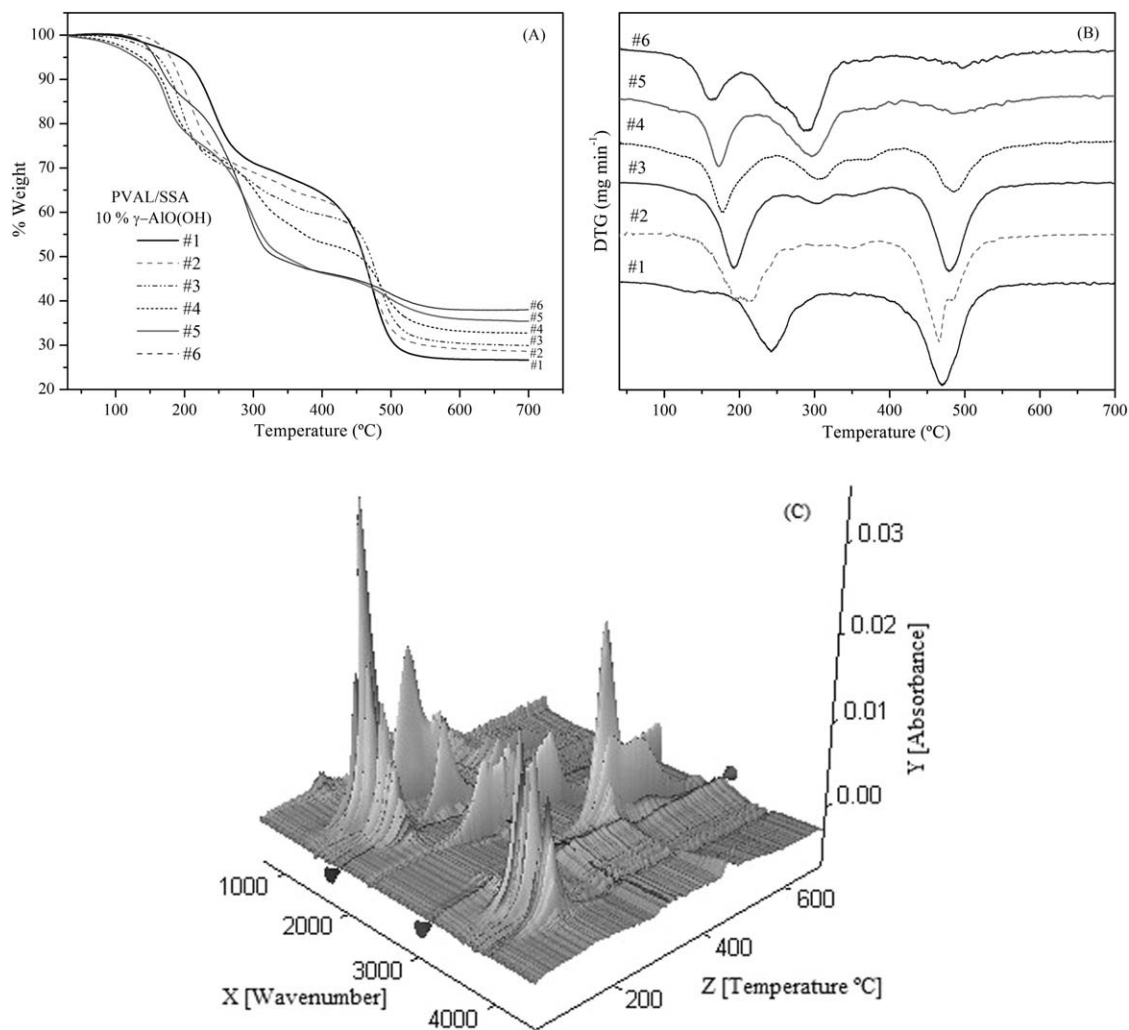
Figure 5. (A) TG, (B) DTG curves for PVAL/SSA membranes loaded with 10% γ-AlO(OH), and (C) three-dimensional graph of absorbance versus wavenumber versus temperature for membrane #4 loaded with 10% boehmite.

reduction of the weight loss at around 480°C, and it can be observed clearly in the DTG curves. The remaining contents, upon reaching 700°C increased with increasing SSA content. These thermal analysis allowed to observe that the membranes loaded with nanoparticules are as thermally stable as the unloaded ones.

Through TG analyser coupled with an infrared spectrometer were obtained the PVAL/SSA membrane #4 loaded with 10% boehmite spectra, which are shown in Figure 5(C). The membrane analyzed presented a first weight loss at around 200°C, corresponding to absorption bands of —OH stretching at 3200–3400 cm^{-1} and O—H angular deformation at 1620–1640 cm^{-1}, both related to free water molecules. At 300°C the absorption bands at 1000–1240 cm^{-1} are related to symmetric and asymmetric stretching of —SO$_3$H group. At the same temperature, the absorption band at 2300–2400 cm^{-1} indicates the presence of CO$_2$, which can be the result of SSA decomposition and polymer degradation. Above 450°C, the absorption bands in the spectrum at 3000–2900 cm^{-1} are related to carbon and hydrogen stretching and bands with low absorption between 1000

and 1200 cm^{-1} are related to O=S—O stretching[11,38] resulting from the membrane decomposition. This analysis indicates that membranes are thermally stable up to 200°C, corroborating with TGA data and that the presence of nanoparticles did not change the membrane thermal stability.

Water Uptake Tests and Mechanical Properties

Water uptake is an important property to proton conductivity, since it is strongly dependent on the membrane water content. Membrane hydrophilicity increases with SSA content because of the presence of a sulfonic acid group, whereas crosslinking also increases with SSA content limiting the membrane water swelling.[11,38] Experimentally, the water uptake decreases as the SSA content was increased (Table II), indicating that the crosslinking is the dominant effect. The presence of nanoparticles can contribute to improving the mechanical and chemical properties of the membranes preventing excessive swelling. The water uptake of unloaded PVAL/SSA membranes is higher as compared to boehmite-loaded PVAL/SSA membranes and the water uptake decreases as the boehmite load increases in the membranes. This effect is probably related to the interaction between the

Table II. Total of Water Uptake in 1 g of Membrane (*Water*), free and Frozen Bound Water Quantity (*Free water*) and Nonfrozen Bound Water Quantity (*Bound water*) to Indicated Membranes

Membrane code	Boehmite content								
	0%			5%			10%		
	Water	Free water	Bound water	Water	Free water	Bound water	Water	Free Water	Bound water
#1	3.82 ± 0.22	3.42 ± 0.12	0.40 ± 0.12	1.80 ± 0.10	1.19 ± 0.07	0.61 ± 0.07	1.51 ± 0.04	0.98 ± 0.04	0.53 ± 0.04
#2	2.39 ± 0.12	1.81 ± 0.06	0.58 ± 0.06	1.69 ± 0.03	1.06 ± 0.03	0.63 ± 0.03	1.28 ± 0.21	0.91 ± 0.10	0.37 ± 0.10
#3	1.54 ± 0.03	0.75 ± 0.02	0.79 ± 0.02	1.46 ± 0.09	0.53 ± 0.07	0.93 ± 0.07	1.20 ± 0.13	0.62 ± 0.08	0.58 ± 0.08
#4	1.59 ± 0.03	0.55 ± 0.02	1.04 ± 0.04	1.18 ± 0.02	0.84 ± 0.03	0.34 ± 0.03	0.83 ± 0.03	0.36 ± 0.03	0.47 ± 0.03
#5	0.98 ± 0.04	0.19 ± 0.03	0.79 ± 0.03	0.78 ± 0.04	0.45 ± 0.03	0.33 ± 0.03	0.69 ± 0.05	0.50 ± 0.03	0.19 ± 0.03
#6	0.65 ± 0.07	0.39 ± 0.06	0.26 ± 0.06	0.65 ± 0.05	0.30 ± 0.03	0.35 ± 0.03	0.79 ± 0.05	0.30 ± 0.04	0.49 ± 0.04

Obs: units of water, free water, and bond water is g per gram of dry membrane.

hydroxyl groups of the PVAL and nanoparticles, which reduces the free volume required for water sorption.

A detailed water state analysis in the prepared membranes is necessary to better understand some membrane properties, as sorption, diffusion, permeation, and transport properties. The absorbed water in hydrophilic polymers has some thermodynamic properties that allows classify it as free water, frozen bound water, and nonfrozen bound water.[35,42] Free water has the same phase transition temperature as bulk water (0°C) and is not intimately bound to the polymer chain. Frozen bound water has a phase transition temperature lower than 0°C and is slightly bound to the polymer or interacts weakly with nonfrozen bound water. Nonfrozen bound water has no detectable phase transition in the temperature range of −80°C to 0°C, and arises from a strong interaction with the polymer chain.[35]

The nonfrozen bound water volume is typically dependent on ionic groups polarity contained in the polymer chain and its contents can influence directly the membranes transport properties. Kim et al. showed that the water state is correlated with the proton conductivity, methanol permeability, and electro-osmotic drag of proton exchange membranes. By reducing the frozen bound and free water content of the poly(arylene ether sulfone)-based copolymers, they were able to reduce the water osmotic drag and methanol permeability of the corresponding membranes. Such attractive membrane characteristics were observed at membranes low water contents as compared to Nafion.[43] Hwang et al. investigated prepared membranes using PVAL grafted with 4-formyl-1,3-benzenedisulfonic acid disodium salt and identified a special microstructural feature without phase separation that enabled an appreciable free water reduction, being the presence of polar groups in the polymer chain allowed by large nonfrozen water sorption in the membranes. The large nonfrozen bound water sorption was the main reason for the attractive DMFC membrane characteristics and a detailed analysis of the water state revealed that the connected system of narrow water channels permitted a low methanol permeation with high mobility of protonic charge carriers.[42] In this study, the quantity of nonfrozen bound water in the membranes PVAL/SSA loaded and unloaded with boehmite nanoparticles was determined using DSC measurements and the results are shown in Table II.

The data in the Table II show that the content of free water and nonfrozen bound water in the membranes is dependent on the SSA content. In most cases two ice melting peaks were observed in the DSC curves, being at the lower temperature associated with frozen water bound to polar and ionic groups and at 0°C associated free water or freezable water, both were accounted for as free water and the value is shown in the Table II. The nonfrozen bound water amount inside the membranes increases with the increasing of SSA in the membranes, because of the insertion of high polarity groups (i.e., —SO₃H) in the polymer chain. On the other hand, the crosslinking reaction of membranes #4 to #6 decreases the free hydroxyl groups from PVAL, increasing the polymer rigidity and consequently decreasing the nonfrozen bound water content in the membranes.

In the membranes loaded with boehmite nanoparticles the fraction of nonfrozen bound water in the most instances was higher

Table III. Modulus of Elasticity to Indicate Membranes PVAL/SSA Unloaded and Loaded with Boehmite Nanoparticles

| | Boehmite content | | |
Membrane code	0% E (MPa)	5% E (MPa)	10% E (MPa)
#1	10.9	40.8	70.8
#3	17.4	17.3	18.9
#4	30.2	25.7	47.8
#6	4.00	287	140

than in the unloaded membranes, probably due to the presence of nonfrozen water adsorbed in the boehmite nanoparticles. However, from the membranes #3 can be observed a decreasing in the nonfrozen bound water quantity, which may be explained by the increasing of the crosslinking reaction degree with consequent increasing of the polymer rigidity. And also by an interaction between nanoparticles and polymer chain resulting in the decreasing of the polymer free volume, being this effect more pronounced on the membranes loaded with 5% of boehmite nanoparticles. The water uptake tests allowed to observe that the nanoparticles presence inside the membranes prevented membranes swelling; on the other hand, the presence of higher quantity of nonfrozen bound water in the membranes loaded with boehmite nanoparticles can improve the transport properties through the membrane.

The mechanical properties of the membranes were evaluated by DMA equipment, and was determined the modulus of elasticity or Young's modulus, that enabled to verify the materials stiffness. Table III shows the Young's modulus of the PVAL/SSA membranes unloaded and loaded with boehmite nanoparticles. The Young's modulus values of the membranes without boehmite increased with the raise of SSA concentration. Probably, the augmentation of acid concentration induces the formation of greater crosslinking, requiring higher tension to cause the same deformation in the membrane and indicating higher stiffness. In most cases, water molecules in the polymers behave as

plasticizers, facilitating the movement between chains. In this case, it is suggested that the lower water absorption, with increasing of the acid concentration, also contributes to increase the membrane stiffness.

Table III shows that the membranes mechanical properties improved with the nanoparticles loading. In most cases, the PVAL/SSA membranes loaded with boehmite presented greater Young's modulus than the ones unloaded and this effect is probably due to interactions between boehmite nanoparticles and the functional groups of the polymer and the SSA that make the polymer chains more rigid. The low water absorption in the membranes loaded with nanoparticles may also have contributed to their self high value of Young's modulus. All membranes #6 exhibited a different behavior from the other membranes; however, the presence of the nanoparticles in the membrane composition resulted in the increasing of the Young's modulus. On the other hand, the membranes #6 deformation loaded with nanoparticles under tension is too small breaking after a short time, indicating fragility.

Ion Exchange Capacity

The IEC indicates the density of ionizable hydrophilic groups in the membrane polymer matrix that are responsible for the ionic conductivity of the membrane. The IEC values increase [Figure 6(A)] with the SSA content in the polymer chain. This is because the SSA contains a fixed sulfonic acid group. Figure 6(B) shows the calculated IEC values required for the neutralization of one and two protons of the SSA and the experimental IEC values obtained for the different membranes. The results suggest that there is not a complete crosslinking between the SSA molecules and the PVAL polymer. The presence of unreacted carboxylic acid groups from the SSA contributes to a high IEC and thus the IEC values are higher than expected and it may be an indicative of high protonic conductivity. The IEC values corroborate with FTIR and indicate that a partial crosslinking between PVAL and SSA had occurred. The crosslinking control was done through heat treatment, 90°C for 1.5 h, to which membranes were submitted to during the preparation procedure.
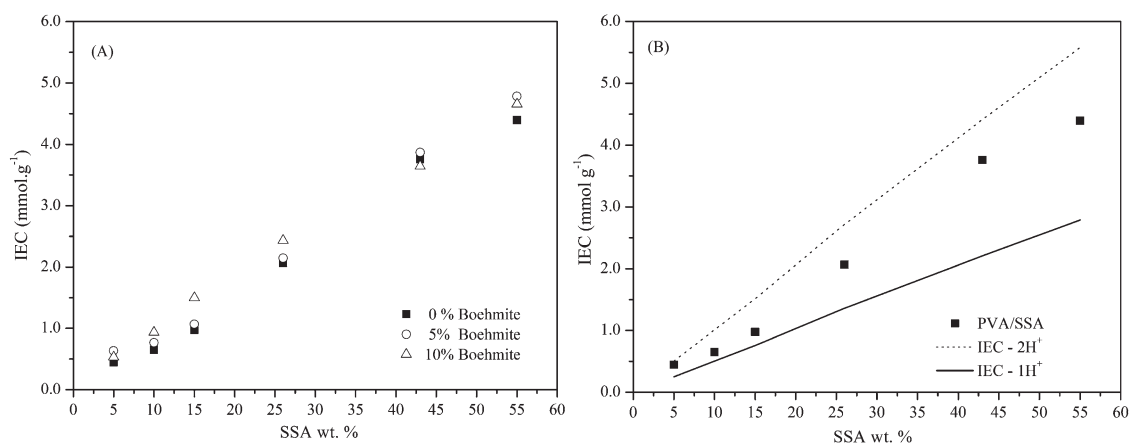

Figure 6. (A) IEC versus SSA wt % for PVAL/SSA membranes loaded and unloaded with boehmite nanoparticles and (B) IEC versus %SSA for PVAL/SSA membrane and IEC calculated value for one proton (IEC-1H$^+$) and two protons (IEC-2H$^+$).

Table IV. Results of Permeability (P), Proton Conductivity by Two-Probe Technique (σ) and Proton Conductivity After Assembling the Electrodes in a Fuel Cell (σ^*) for Membranes PVAL/SSA Loaded and Unloaded with Boehmite Nanoparticles

Membrane code	Boehmite content							
	0%		5%			10%		
	P	σ	P	σ	σ^*	P	σ	σ^*
	10^{-13} mol cm bar^{-1} s^{-1} cm^{-2}	10^{-2} S cm^{-1}	10^{-13} mol cm bar^{-1} s^{-1} cm^{-2}	10^{-2} S cm^{-1}	10^{-2} S cm^{-1}	10^{-13} mol cm bar^{-1} s^{-1} cm^{-2}	10^{-2} S cm^{-1}	10^{-2} S cm^{-1}
#1	–	0.43±0.03	–	0.05±0.01	–	–	0.07±0.04	–
#2	–	0.82±0.04	–	0.35±0.09	–	–	0.10±0.00	–
#3	–	1.03±0.13	–	0.67±0.11	–	–	0.52±0.11	–
#4	8.09±0.21	2.00±0.08	6.23±0.13	2.74±0.23	1.86±0.08	3.47±0.02	1.64±0.18	1.50±0.09
#5	1.10±0.16	5.69±0.11	1.14±0.24	4.34±0.17	–	8.85±0.11	4.59±0.11	1.98±0.07
#6	–	6.33±0.20	7.67±0.33	4.21±0.04	–	3.03±0.09	5.92±0.09	4.81±0.10

Proton Conductivity

Table IV shows the proton conductivity data (σ), obtained by the two-probe technique of the unloaded and boehmite-loaded PVAL/SSA membranes at 25°C. Proton conductivities are in the range of 5×10^{-4} S cm^{-1} to 6×10^{-2} S cm^{-1}. The water content in membranes to operate at low PEMFC temperature (below 90°C) is of relevance to infer the proton conductivity. However, the overall effect observed in Table IV is that the proton conductivity is mostly controlled by the SSA presence, once the water represents about 70 wt % of membrane weigh (Table II) in all cases; and added to it, the fuel cell experiments were performed at 100% relative humidity. As mentioned before, higher SSA concentrations in the PVAL increase crosslinking and decrease swelling, but higher sulfonic acid concentration and special microstructural features without phase separation facilitate the proton conductivity. The addition of nanoparticles in membranes with a moderate to high SSA concentration has a minor effect on the proton conductivity. However, the presence of nanoparticles, which are not proton conductors, in the membranes with low SSA concentrations, reduces the free volume for water uptake and impair the proton mobility inside the membrane leading to lower proton conductivity values.

PEMFC Tests

The membranes that presented the highest proton conductivity values in the two-probe tests (Table IV) were submitted to the fuel cell and permeability testing, being the fuel cell testing performed only on the membranes loaded with boehmite nanoparticles. Only certain membranes presented mechanical resistance when inserted in a fuel cell, corroborating with performance of membranes in the mechanical resistance tests showed in the Table III. The proton conductivity ($^*\sigma$) for the prepared membranes, after assembling the electrodes, in a fuel cell and their permeability to hydrogen (P) obtained using the time-lag method are shown in the Table IV. The thicknesses of membranes tested in this study were: Nafion with 125 μm; membrane #4 with 5% of boehmite 133 μm; the membrane #4 with 10% of boehmite 101 μm; the membrane #5 with 10% of boehmite 164 μm and membrane #6 with 10% of boehmite 199 μm. Proton conductivity for all the membranes increased with SSA concentration. It can be observed proton conductivity ranges between 1.5×10^{-2} S cm^{-1} and 4.8×10^{-2} S cm^{-1}; Nafion under the same conditions has a proton conductivity of 5.7×10^{-2} S cm^{-1}. The proton conductivity of these membranes were higher than other PVAL composite membranes related in the Refs. 26, 44. An increase in the nanoparticles load causes a small decrease in the proton conductivity, according to the proton conductivity of membranes determined by two-probe technique shown in Table IV. The hydrogen permeation results for membranes tested are slightly lower than Nafion that has the hydrogen permeation of 833×10^{-12} mol cm bar^{-1} s^{-1} cm^{-2}, and the results are shown in the Table IV. It was observed a rise in the proton conductivity to membranes that showed higher permeability to hydrogen and higher water uptake values.

Figure 7 shows that increasing the boehmite content above 5 wt % resulted in a decrease in the PEMFC performance, which leads to a decrease in the maximum current density (310–289 mA cm^2) and power peak (80–69 mW cm^2). The decrease in
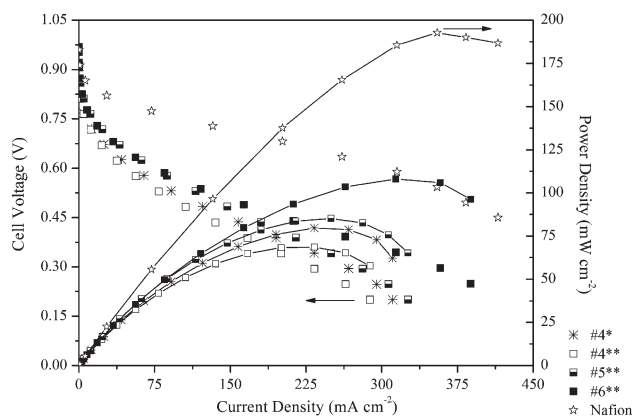
Figure 7. Polarization curves for the PEMFC using the PVAL/SSA membranes indicated, #4* loaded with 5 wt % boehmite and #4**, #5**, and #6** loaded with 10 wt % boehmite and the Nafion 115.

the PEMFC performance with the increase in the boehmite load is probably related to the decreasing of the membrane proton conductivity (Table IV). On the other hand, increasing the SSA content leads to a better performance because the proton conductivity also increases.

Comparing the best performing membrane, membrane #6 loaded with 10 wt % of boehmite, with Nafion 115 it can be concluded that Nafion exhibits a maximum power density about two times greater than this membrane. This result can be explained by the slightly higher proton conductivity (Table IV) and lower thickness of the Nafion membrane, about 125 μm, as compared with 200 μm of membrane #6 loaded with 10 wt % of boehmite. Although the membranes have presented a lower performance and were more fragile than the Nafion membrane, the results obtained were great and very promising for using as PEMFC, once low cost materials were used to prepare the membranes. Further developments should target the improvement of the mechanical properties of these membranes.

CONCLUSIONS

PVAL/SSA membranes unloaded and loaded with boehmite nanoparticles were prepared and evaluated as PEMs for PEMFC applications. The results showed that PVAL/SSA loaded with boehmite can be successfully used in fuel cells fueled with hydrogen. The membrane properties were strongly dependent on the SSA content both as a crosslinking agent and as a donor of hydrophilic SO_3H groups. The proton conductivity values for the PVAL/SSA/boehmite prepared membranes were in the range of 1.5×10^{-2} S cm^{-1} to 4.8×10^{-2} S cm^{-1} and the hydrogen permeability between 3.7×10^{-13} and 4.16×10^{-12} mol cm bar^{-1} s^{-1} cm^{-2}. Both results are comparable with Nafion 115 membrane that exhibited proton conductivity and hydrogen permeability of 5.7×10^{-2} S cm^{-1} and 8.3×10^{-12} mol cm bar^{-1} s^{-1}, respectively.

When inserted in a PEMFC the prepared membrane #6 loaded with 10 wt % of boehmite has performed equivalently to Nafion 115, taking into consideration the membranes thickness ratio, and showed to be very stable. PVAL/SSA membranes loaded with 10 wt % of boehmite indicated to be a very promising

material with attractive cost that should be further investigated, and that should be addressed, especially to mechanical strength.

REFERENCES

1. Kreuer, K. D. *J. Membrane Sci.* **2001**, *185*, 29.

2. Bauer, F.; Denneler, S.; Willert-Porada, M. *J. Polym. Sci. Polym. Phys.* **2005**, *43*, 786.

3. Roziere, J.; Jones, D. *J. Ann. Rev. Mater. Res.* **2003**, *33*, 503.

4. Park, J.-Y.; Kim, T.-H.; Kim, H. J.; Choi, J.-H.; Hong, Y. T. *Int. J. Hydrogen Energy* **2012**, *37*, 2603.

5. Conceição, T. F.; Bertolino, J. R.; Barra, G. M. O.; Pires, A. T. N. *Mater. Sci. Eng. C* **2009**, *29*, 575.

6. Roeder, J.; Zucolotto, V.; Shishatskiy, S.; Bertolino, J. R.; Nunes, S. P.; Pires, A. T. N. *J. Membrane Sci.* **2006**, *279*, 70.

7. Li, H.; Wu, J.; Zhao, C.; Zhang, G.; Zhang, Y.; Shao, K.; Xu, D.; Lin, H.; Han, M.; Na, H. *Int. J. Hydrogen Energy* **2009**, *34*, 8622.

8. Lin, H.; Zhao, C.; Cui, Z.; Ma, W.; Fu, T.; Na, H.; Xing, W. *J. Power Sources* **2009**, *193*, 507.

9. Park, K. T.; Chun, J. H.; Kim, S. G.; Chun, B.-H.; Kim, S. H. *Int. J. Hydrogen Energy* **2011**, *36*, 1813.

10. Bhavani, P.; Sangeetha, D. *Energy* **2011**, *36*, 3360.

11. Rhim, J.-W.; Park, H. B.; Lee, C.-S.; Jun, J.-H.; Kim, D. S.; Lee, Y. M. *J. Membrane Sci.* **2004**, *238*, 143.

12. Tseng, C.-Y.; Ye, Y.-S.; Kao, K.-Y.; Joseph, J.; Shen, W.-C.; Rick, J.; Hwang, B.-J. *Int. J. Hydrogen Energy* **2011**, *36*, 11936.

13. Asensio, J. A.; Gómez-Romero, P. *Fuel Cells* **2005**, *5*, 336.

14. Li, Q.; Jensen, J. O.; Savinell, R. F.; Bjerrum, N. *J. Prog. Polym. Sci.* **2009**, *34*, 449.

15. Pivovar, B. S.; Wang, Y.; Cussler, E. L. *J. Membrane Sci.* **1999**, *154*, 155.

16. Rhim, J.-W.; Yeom, C.-K.; Kim, S.-W. *J. Appl. Chem.* **1998**, *68*, 1717.

17. Jones, D. J.; Roziere, J. Fundamentals, Technology and Applications; In Handebook of Fuel Cells; Gasteiger, H. A., Lamm, A., Vielstich, W., Yokokawa, H., Eds.; Wiley; Hardcover; **2003**.

18. Navarra, M. A.; Croce, F.; Scrosati, B. *J. Mater. Chem.* **2007**, *17*, 3210.

19. Yang, C.-C.; Chien, W.-C.; Li, Y. J. *J. Power Sources* **2010**, *195*, 3407.

20. Yang, C.-C. *J. Membrane Sci.* **2007**, *288*, 51.

21. Amjadi, M.; Rowshanzamir, S.; Peighambardoust, S. J.; Hosseini, M. G.; Eikani, M. H. *Int. J. Hydrogen Energy* **2010**, *35*, 9252.

22. Saccà, A.; Gatto, I.; Carbone, A.; Pedicini, R.; Passalacqua, E. *J. Power Sources* **2006**, *163*, 47.

23. Kozawa, Y.; Suzuki, S.; Miyayama, M.; Okumiya, T.; Traversa, E. *Solid State Ionics* **2010**, *181*, 348.

24. Qian, W.; Shang, Y.; Fang, M.; Wang, S.; Xie, X.; Wang, J.; Wang, W.; Du, J.; Wang, Y.; Mao, Z. *Int. J. Hydrogen Energy* **2012**, *37*, 12919.

25. Alberti, G.; Casciola, M.; Pica, M.; Tarpanelli, T.; Sganappa, M. *Fuel Cells* **2005**, *5*, 366.

26. Kim, D. S.; Park, H. B.; Rhim, J. W.; Moo Lee, Y. *J. Membrane Sci.* **2004**, *240*, 37.

27. Thiam, H. S.; Daud, W. R. W.; Kamarudin, S. K.; Mohammad, A. B.; Kadhum, A. A. H.; Loh, K. S.; Majlan, E. H. *Int. J. Hydrogen Energy* **2011**, *36*, 3187.

28. Kim, S.-M.; Lee, Y.-J.; Jun, K.-W.; Park, J.-Y.; Potdar, H. S. *Mater. Chem. Phys.* **2007**, *104*, 56.

29. Boumaza, A.; Favaro, L.; Lédion, J.; Sattonnay, G.; Brubach, J. B.; Berthet, P.; Huntz, A. M.; Roy, P.; Tétot, R. *J. Solid State Chem.* **2009**, *182*, 1171.

30. Suzuki, F.; Onozato, K.; Kurokawa, Y., *J Appl Chem* **1990**, *39*, 371.

31. Özdilek, C.; Kazimierczak, K.; van der Beek, D.; Picken, S. J., *Polymer* **2004**, *45*, 5207.

32. Halbach, T. S.; Mülhaupt, R., *Polymer* **2008**, *49*, 867.

33. Monti, M.; Camino, G., *Polym Degrad Stab* **2013**, *98*, 1838.

34. Zhang, J.; Ji, Q.; Zhang, P.; Xia, Y.; Kong, Q. *Polym. Degrad. Stab.* **2010**, *95*, 1211.

35. Ping, Z. H.; Nguyen, Q. T.; Chen, S. M.; Zhou, J. Q.; Ding, Y. D. *Polymer* **2001**, *42*, 8461.

36. Tomé, L. C.; Gonçalves, C. M. B.; Boaventura, M.; Brandão, L.; Mendes, A. M.; Silvestre, A. J. D.; Neto, C. P.; Gandini, A.; Freire, C. S. R.; Marrucho, I. M. *Carbohyd Polym.* **2011**, *83*, 836.

37. Kim, D. S.; Guiver, M. D.; Nam, S. Y.; Yun, T. I.; Seo, M. Y.; Kim, S. J.; Hwang, H. S.; Rhim, J. W. *J. Membrane Sci.* **2006**, *281*, 156.

38. Lee, D. K.; Lee, K. J.; Kim, Y. W.; Kim, J. H. *Desalination* **2008**, *233*, 104.

39. Buzzoni, R.; Bordiga, S.; Ricchiardi, G.; Spoto, G.; Zecchina, A. *J. Phys. Chem.* **1995**, *99*, 11937.

40. Mansur, H. S.; Sadahira, C. M.; Souza, A. N.; Mansur, A. A. P. *Mater. Sci. Eng. C* **2008**, *28*, 539.

41. Mallapragada, S. K.; Peppas, N. A.; Colombo, P. *J. Biomed. Mater. Res.* **1997**, *36*, 125.

42. Hwang, B.-J.; Joseph, J.; Zeng, Y.-Z.; Lin, C.-W.; Cheng, M.-Y. *J. Membrane Sci.* **2011**, *369*, 88.

43. Kim, Y. S.; Dong, L.; Hickner, M. A.; Glass, T. E.; Webb, V.; McGrath, J. E. *Macromolecules* **2003**, *36*, 6281.

44. Yang, C.-C. *Int. J. Hydrogen Energy* **2011**, *36*, 4419.